DOI: 10.1142/S0219530519410112



Adaptive display images

Meipeng Zhi

School of Mathematics, Guangdong Provincial Key Lab of Computational Science, Sun Yat-Sen University Guangzhou 510275, P. R. China 948607184@qq.com

Yuesheng Xu*

Department of Mathematics and Statistics Old Dominion University, Norfolk, Virginia 23529, USA *y1xu@odu.edu

> Received 9 August 2019 Accepted 30 October 2019 Published 6 December 2019

We develop a numerical method for construction of an adaptive display image from a given display image which is an artificial scene displayed in a computer screen. The adaptive display image is encoded on an adaptive pixel mesh obtained by a merging scheme from the original pixel mesh. The cardinality of the adaptive pixel mesh is significantly less than that of the original pixel mesh. The resulting adaptive display image is the best L_p piecewise constant approximation of the original display image. Under the assumption that a natural image, the real scene that we see, belongs to a Besov space, we provide the optimal L_p error estimate between the adaptive display image and its original natural image. Experimental results are presented to demonstrate the visual quality, the approximation accuracy and the computational complexity of the adaptive display image.

Keywords: Image analysis; image processing; approximation algorithms; Besov spaces.

Mathematics Subject Classification 2010: 62H35, 94A08, 68W25, 30H25

1. Introduction

Images play an important role in science, engineering and social activities. A *natural* image is a real scene observed by human eyes. Normally, a natural image is captured by a camera and displayed on a computer screen by using a pixel matrix called a *pixel mesh*. In this paper, we shall refer to the image displayed on a computer screen as a *display image*. It is also called a digital image or an observed image in the literature. In general, a display image corresponds to a pixel mesh which is a uniform

^{*}Corresponding author.

partition of the image domain with a cardinality determined by its resolution. For example, displaying an $n \times n$ display image needs a pixel mesh of cardinality n^2 . We observe that at a portion of the image domain where the pixel values of the image do not change rapidly it may not be necessary to store all the values. This observation motivates us to construct a *non-uniform* pixel mesh, adapted to a given image, which encodes an *adaptive* display image with a significantly less cardinality but preserving the visual quality of the original display image.

The main purpose of this paper is to develop a merging scheme which generates an adaptive pixel mesh from a given uniform pixel mesh of a display image. Based on the adaptive pixel mesh, one can obtain an adaptive display image, which is the best L_p piecewise constant approximation of the original display image on the adaptive pixel mesh. The resulting adaptive display image approximates well the original image and has significantly less cardinality than that of the original image. We provide an analysis of the approximation accuracy of the adaptive display image that approximates the original display image. Mathematically, a natural image is a time-continuous function, and a display image is its piecewise constant approximation on a pixel mesh. In order to study the approximation error of adaptive display images, we consider the $L_p(\mathbb{T})$ error between the adaptive display image and its original natural image under the assumption that a natural image belongs to a Besov space, where \mathbb{T} denotes the domain of a natural image (it is also called the field of view (FOV)). In passing, we point that the proposed merging scheme is in fact a reverse process of the basic dividing scheme discussed in [7, 13, 22, 23] in the context of adaptive wavelet approximation.

We organize this paper in six sections. In Sec. 2, we discuss proper function spaces for measuring the smoothness of natural images and display images. We propose in Sec. 3 the merging scheme for the construction of an adaptive pixel mesh. Section 4 is devoted to analysis of the $L_p(\mathbb{T})$ error between an adaptive display image and its original natural image by assuming that a natural image belongs to a Besov space. In Sec. 5, we present numerical results which demonstrate the visual quality and the approximation accuracy of the resulting adaptive display image. We draw conclusions in Sec. 6.

2. Natural Images and Besov Spaces

We first discuss natural images. A natural image is a scene that a human being sees by his or her eyes. Mathematically, it is a 2D time-continuous intensity function of a projection of a 3D scene in the real world, whose values represent the brightness or the number of proton of a point of the scene, [16]. Values of a natural image are bounded if light sources are not considered. Besides, most of natural images in the real world consist of some smooth regions separated by edges. It seems that for a common sense, the more edges it has, the less "smooth" it is. The smoothness of a natural image is an important characteristic, in many applications such as wavelet compression of images and image denoising/deblurring.

In most of cases, we do not know the exact mathematical formulation of natural images. However, we shall assume natural images are locally integrable so that we can "observe" them by some devices, such as cameras. We call this "observed" image the display image. A display image is an artificial scene showed in a display device, which is a piecewise constant approximation of its natural image.

What kind of functions can we use to represent natural images? In other words, what kind of function spaces do natural images belong to? This is a long standing interesting research problem. Since the natural image is supposed to be locally integrable and has a bounded domain, the first space that one may consider is the $L_p(\mathbb{T})$ space. Recall that for the FOV $\mathbb{T} := [0,1] \times [0,1]$ of natural images (or display images), the $L_p(\mathbb{T})$ space, 0 , is defined by

$$L_p(\mathbb{T}) := \left\{ f : \|f\|_{L_p(\mathbb{T})} := \left(\int_{\mathbb{T}} |f(\boldsymbol{x})|^p \mathrm{d}\boldsymbol{x} \right)^{1/p} < \infty \right\} \quad 0 < p < \infty,$$

 $L_{\infty}(\mathbb{T}):=\{f:\|f\|_{L_{\infty}(\mathbb{T})}:=\operatorname*{ess\,sup}_{\boldsymbol{x}\in\mathbb{T}}|f(\boldsymbol{x})|<\infty\},$

where $\mathbf{x} := (x_1, x_2)$. In particular, when p = 2, the space $L_2(\mathbb{T})$ is a Hilbert space. For simplicity, when f is defined on \mathbb{T} , its $L_p(\mathbb{T})$ norm is denoted by $||f||_p$. Since we assume a natural image is a bounded time-continuous function, we know that it belongs to $L_{\infty}(\mathbb{T})$. It was indicated in [6] that natural images, belonging to $L_p(\mathbb{T})$, are naturally distributional images and carry more structures than general distributional images, such as the "layer-cake representation" which can be found in [17]. Many medical imaging applications assume that natural images belong to $L_p(\mathbb{T})$, especially $L_2(\mathbb{T})$. This is mainly because these applications (such as magnetic resonance imaging) are related with orthogonal bases, wavelets or the Fourier transform. However, for some specific image processing applications, such as denoising, deblurring or compression, it is often assumed that natural images belong to certain subspaces of $L_p(\mathbb{T})$ (for example, the bounded variation (BV) space and Sobolev spaces), depending upon specific applications.

The total variation (TV) denoising model proposed in [20] is popular among image denoising models. It assumes that natural images belong to the BV space. Functions of the BV space can represent well edges of an image since they contain characteristic functions of simple sets. This is a basic assumption of image restoration, image segmentation, image deconvolution and image compression for which the TV model is used. For piecewise constant noisy display images, the TV model denoises well while preserving sharp edges, although the model has some drawbacks. It was pointed out in [19] that the TV minimization tends to create constant patches in display images and causes the staircase effect. Consequently, the TV model does not always represent well texture or oscillatory details of an image, as it has been analyzed in [18]. Also, it was shown in [1, 15] that natural images are not well represented by functions of BV.

An intrinsic idea is that natural images may belong to more general spaces, such as Besov spaces. Roughly speaking, functions of the Besov space $B_q^{\alpha}(L_p(\mathbb{T}))$ are those that belong to $L_p(\mathbb{T})$ having the α order of smoothness. We now review the definition of Besov spaces (see, for instance [4]). Let \mathbb{Z} denote the set of all integers and \mathbb{R} the set of all real numbers. For $f \in L_p(\mathbb{T})$ and $h \in \mathbb{R}^2$, we define the difference operators by

$$\Delta_{m{h}}^0 f(m{x}) := f(m{x}), \quad \Delta_{m{h}}^{k+1} f(m{x}) := \Delta_{m{h}}^k f(m{x}+m{h}) - \Delta_{m{h}}^k f(m{x}),$$
 $m{x} \in \mathbb{T}, \quad k = 0, 1, \dots,$

where $\Delta_{\boldsymbol{h}}^k f(\boldsymbol{x})$ is defined for $\boldsymbol{x} \in \mathbb{T}_{k\boldsymbol{h}} := \{ \boldsymbol{x} \in \mathbb{T} : \boldsymbol{x} + k\boldsymbol{h} \in \mathbb{T} \}$ with k > 0. For $\alpha > 0$, we choose $r \in \mathbb{Z}$ such that $r - 1 \le \alpha < r$. Then for $\alpha > 0$ and $0 < p, q \le \infty$, the Besov space seminorm is defined by

$$|f|_{B_q^{\alpha}(L_p(\mathbb{T}))} := \left(\int_0^{\infty} [t^{-\alpha}\omega_r(f,t)_p]^q \frac{\mathrm{d}t}{t} \right)^{1/q},$$

with the supremum when $q = \infty$, where $\omega_r(f, t)_p$ is the $L_p(\mathbb{T})$ -modulus of smoothness defined by

$$\omega_r(f,t)_p := \sup_{|\boldsymbol{h}| \le t} \left(\int_{\mathbb{T}_{r\boldsymbol{h}}} |\Delta_{\boldsymbol{h}}^r f(\boldsymbol{x})|^p d\boldsymbol{x} \right)^{1/p},$$

with the usual change to the essential supremum when $p = \infty$. We say a function $f \in B_q^{\alpha}(L_p(\mathbb{T}))$ if $|f|_{B_q^{\alpha}(L_p(\mathbb{T}))} < \infty$. The Besov space norm is

$$||f||_{B_q^{\alpha}(L_p(\mathbb{T}))} := ||f||_p + |f|_{B_q^{\alpha}(L_p(\mathbb{T}))}.$$

In particular, when p=q=2, the Besov space $B_2^{\alpha}(L_2(\mathbb{T}))$ reduces to the Sobolev space $H^{\alpha}(\mathbb{T})$. When $0 < \alpha < 1$, $1 \leq p \leq \infty$ and $q = \infty$, the Besov space $B_{\infty}^{\alpha}(L_p(\mathbb{T}))$ is the Lipschitz space $\text{Lip}(\alpha, L_p(\mathbb{T}))$.

It is well-documented in [4, 5, 8–10] that performance of wavelet-based image processing algorithms in many image processing applications was analyzed under the assumption that natural images belong to Besov spaces. In [14], the BV space and generalized homogeneous Besov spaces were used to decompose a display image into a piecewise smooth component and an oscillatory component (texture or noise). A theory for analyzing errors of the wavelet compression of display images was introduced in [8], based on the assumption that natural images belong to a class of Besov spaces $B_q^{\alpha}(L_q(\mathbb{T}))$, $0 < \alpha < 1$, p > 0, $1/q = \alpha/2 + 1/p$. Furthermore, according to this theory, it was indicated that display images have the same order of smoothness as their natural images, and it was strongly suggested that the order of smoothness of natural images and display images ranges from 0.3 to 0.6 which can be estimated by the wavelet compression method. Natural images were considered in [4] to belong to Besov spaces $B_q^{\alpha}(L_q(\mathbb{T}))$, $0 < \alpha < 1, 1/q = \alpha/2 + 1/2$, of minimal order of smoothness, embedded in $L_2(\mathbb{T})$. An experiment presented there used the wavelet compression method to estimate the order of smoothness of a class of 24 display images, and the numerical results suggest that the order of smoothness of many natural images and display images ranges from 0.3 to 0.7. It was assumed in [3] that natural images belong to the Besov space $B_{\infty}^{\alpha}(L_2(\mathbb{T}))$, with $0 < \alpha < 1$,

instead of $BV(\mathbb{T})$, for the purpose of image deblurring, and it was shown that most of natural images are not of BV space and a rich class of natural images and display images belong to $B_{\infty}^{\alpha}(L_2(\mathbb{T}))$ or $B_{\infty}^{\gamma}(L_1(\mathbb{T})) \cap B_{\infty}^{\beta}(L_2(\mathbb{T}))$, with $0.2 < \gamma, \beta < 0.7$. Since Besov spaces can characterize the order of smoothness of natural images and their multiscale nature, it is wildly accepted that functions of Besov spaces can well represent natural images.

In this paper, we adopt the assumption that natural images belong to Besov spaces $B_{\tau}^{\alpha+\varepsilon}(L_v(\mathbb{T}))$, $1 , <math>0 < \alpha < \alpha + \varepsilon \leq \min(1, 2-2/p)$ with $\varepsilon > 0$, $p \leq v \leq \infty$ and $0 < \tau \leq \infty$. In fact, $B_{\tau}^{\alpha+\varepsilon}(L_v(\mathbb{T}))$ is continuously embedded in $B_q^{\alpha}(L_q(\mathbb{T})), \ 0 < \alpha < 1, \ 1/q = \alpha/2 + 1/p, \ \text{and it contains} \ B_{\tau}^{\alpha+\varepsilon}(L_2(\mathbb{T})) \ \text{when} \ p = 2.$ In what follows, for simplicity, we use $B_{p,q}^{\alpha}$ to denote the Besov space $B_q^{\alpha}(L_p(\mathbb{T}))$. In the mean time, we use $|\cdot|_{B^{\alpha}_{p,q}}$ and $|\cdot|_{B^{\alpha}_{p,q}}$ to represent the seminorm and the norm of Besov space $B_{p,q}^{\alpha}$, respectively.

3. Construction of Adaptive Display Images

In this section, we describe a merging scheme which is used to generate an adaptive pixel mesh from the pixel mesh of a given display image for construction of an adaptive display image. The resulting adaptive display image is the best L_p piecewise constant approximation of its original display image on the adaptive pixel mesh.

A display image, displayed on a computer screen, is an approximation of a natural image. It is stored as an $n \times m$ matrix in the bitmap format. For simplicity, in this paper we consider gray-scale images and assume that n=m. Each entry of this matrix is a pixel value, which is sampled by a measuring device such as a charge coupled device (CCD) or a complementary metal oxide semiconductor (CMOS) camera. These cameras use optical lens to project objective scenes onto smaller ones which can be covered by camera sensors. The range of the smaller scene is the FOV. We assume that sensors of the cameras have $n \times n$ sensing units (or camera pixels), each of which is related to a sensitivity function and a sensing area. The sensing units capture the corresponding pixel values in the same time and store the sample data in the memory. In general, screens of display devices are formed by display pixel matrices. Each display pixel is a small rectangle, and the color displayed by each pixel is depending on the corresponding pixel value. When the computer receives an operation to show a display image, it will get pixel values of the corresponding matrix from the memory. Then the computer will use $n \times n$ display pixels to show the display image. If the display pixel is small enough, we cannot distinguish between the display image and its natural image by our eyes. For more details of display images, readers are referred to [16].

We now review a mathematical model of display images. Throughout this paper, we shall use f to denote a generic function while use u to represent a natural image and u_n to represent its display image with a resolution level n. Let N denote the set of the natural numbers and \mathbb{N}_+ the set of positive integers. For $n \in \mathbb{N}_+$, we set $\mathbb{Z}_n := \{0, 1, \dots, n-1\}.$ For a set \mathbb{A} , we let $\mathbb{A}^2 := \mathbb{A} \otimes \mathbb{A}$, where \otimes denotes the tensor product. We divide \mathbb{T} into $n \times n$ equal size display pixels

$$\mathbb{T}_{\pmb{j}}^{(n)} := \left[\frac{j_1}{n}, \frac{j_1+1}{n}\right] \times \left[\frac{j_2}{n}, \frac{j_2+1}{n}\right],$$

where $\mathbf{j} := (j_1, j_2) \in \mathbb{Z}_n^2$ is the position of a pixel. We call $\mathfrak{T}^n := \{\mathbb{T}_{\mathbf{j}}^{(n)}\}_{\mathbf{j} \in \mathbb{Z}_n^2}$ the pixel mesh with a resolution level n. For a natural image $u \in L_p(\mathbb{T}), 0 , the pixel value <math>u_{\mathbf{j}}$ captured by a sensing unit at the position \mathbf{j} can be evaluated by

$$u_{\boldsymbol{j}} := \int_{\mathbb{T}^{(n)}_{\boldsymbol{j}}} s_{\boldsymbol{j}}^{(n)}(\boldsymbol{x}) u(\boldsymbol{x}) \mathrm{d}\boldsymbol{x},$$

where $s_{j}^{(n)}$ is the sensitivity function at pixel $\mathbb{T}_{j}^{(n)}$. The sensitivity function of a CCD camera is well modeled by averaging the natural image u over the sensing area. Thus, we can rewrite the pixel value as

$$u_{j} = \frac{1}{|\mathbb{T}_{j}^{(n)}|} \int_{\mathbb{T}_{j}^{(n)}} u(\boldsymbol{x}) d\boldsymbol{x}, \tag{3.1}$$

where $|\mathbb{T}_{j}^{(n)}|$ is the area of $\mathbb{T}_{j}^{(n)}$. Note that u_{j} is bounded, which means $|u_{j}| < \infty$, due to $u \in L_{p}(\mathbb{T})$. For a square $\mathbb{Q} \subset \mathbb{T}$ and $x \in \mathbb{R}^{2}$, we define the characteristic function $\chi_{\mathbb{Q}}(x)$ of \mathbb{Q} by

$$\chi_{\mathbb{Q}}(\boldsymbol{x}) := egin{cases} 1, & \boldsymbol{x} \in \mathbb{Q}, \\ 0, & \text{otherwise}. \end{cases}$$

Here, we assume that the display pixel is a little square and has the same size as the camera pixel. The display image u_n can then be represented by a piecewise constant function determined via pixel values u_j computed by (3.1) through the formula

$$u_n(\boldsymbol{x}) := \sum_{\boldsymbol{j} \in \mathbb{Z}^2} u_{\boldsymbol{j}} \chi_{\mathbb{T}_{\boldsymbol{j}}^{(n)}}(\boldsymbol{x}), \quad \boldsymbol{x} \in \mathbb{T}.$$
(3.2)

Note that the display image model (3.2) was also used in [4, 8] for analyzing errors of the wavelet compression for images, where the display image is called "observed image".

In practice, displaying a display image with a resolution level n needs a pixel mesh with cardinality n^2 . When n is large, n^2 is huge and as a result it will require a large amount of computing time to process the image. Do we really need n^2 pixels? Can we construct an approximate image of a display image such that the cardinality of its pixel mesh is significantly less than that of the original pixel mesh, and its visual quality is comparable to that of the original display image? We provide an answer to these questions.

We first describe a merging scheme for the design of the adaptive pixel mesh. To this end, we define necessary notation. For $\mathbb{Q} \subset \mathbb{T}$ and $f \in L_p(\mathbb{Q})$, 0 ,

we denote by $\mathscr{C}_{\mathbb{Q}}^p f: L_p(\mathbb{Q}) \to \mathbb{R}$ the best L_p constant approximation of f on \mathbb{Q} . We define the L_p local error of f on \mathbb{Q} by

$$E(f, \mathbb{Q})_p := \|f - \mathscr{C}_{\mathbb{Q}}^p f\|_{L_p(\mathbb{Q})}.$$

It can be seen easily from the definition of local error $E(f,\mathbb{Q})_p$ that for any $\mathbb{Q} \subset$ $\mathbb{Q}' \subset \mathbb{T}$ and $f \in L_p(\mathbb{T})$, the following inequality holds:

$$E(f, \mathbb{Q})_p \le E(f, \mathbb{Q}')_p. \tag{3.3}$$

For simplicity, we use $\mathbb{T}^k_{\boldsymbol{j}}$ to denote a pixel at position \boldsymbol{j} with size $\frac{2\pi}{2^k} \times \frac{2\pi}{2^k}$. We define the parent pixel of $\mathbb{T}^k_{\boldsymbol{j}}$ by $\mathbf{P}^k_{\boldsymbol{j}} := \mathbb{T}^{k-1}_{(\lfloor \frac{j_1}{2} \rfloor, \lfloor \frac{j_2}{2} \rfloor)}$ in the sense that $\mathbb{T}^k_{\boldsymbol{j}} \subset \mathbb{T}^{k-1}_{(\lfloor \frac{j_1}{2} \rfloor, \lfloor \frac{j_2}{2} \rfloor)}$. In the mean time, we say that \mathbb{T}^k_j is a children pixel of $\mathbb{T}^{k-1}_{(\lfloor \frac{j_1}{2} \rfloor, \lfloor \frac{j_2}{2} \rfloor)}$. The set of children pixels of \mathbb{T}_{i}^{k} is denoted by

$$\mathbf{C}^k_{\boldsymbol{j}} := \Big\{ \mathbb{T}^{k+1}_{(2j_1,2j_2)}, \mathbb{T}^{k+1}_{(2j_1+1,2j_2)}, \ \mathbb{T}^{k+1}_{(2j_1,2j_2+1)}, \mathbb{T}^{k+1}_{(2j_1+1,2j_2+1)} \Big\}.$$

Moreover, if two pixels have the same parent pixel, we say that they are brother pixels. For the brother pixels of \mathbb{T}_{j}^{k} , one can obtain the parent pixel of \mathbb{T}_{j}^{k} first and then find its children pixels. In other words, the set of the brother pixels of \mathbb{T}_i^k can be obtained by

$$\mathbf{B}^k_{\boldsymbol{j}} := \mathbf{C}^{k-1}_{(\lfloor \frac{j_1}{2} \rfloor, \lfloor \frac{j_2}{2} \rfloor)} \Big\backslash \{\mathbb{T}^k_{\boldsymbol{j}}\}.$$

Note that each pixel has only one parent pixel, four children pixels and three brother pixels.

The merging scheme merges brother pixels into their parent pixel based on the L_p local error of the display image on those pixels and an input parameter δ , called the global error. We denote by \mathcal{M}_{δ} the adaptive pixel mesh generated by the merging scheme with the global error δ . Each pixel $\mathbb{Q} \in \mathcal{M}_{\delta}$ is called an adaptive pixel. Note that an adaptive pixel is a square. If the L_p local error of a display image on a pixel is less than or equal to δ but the L_p local error on the corresponding parent pixel is larger than δ , then this pixel is an adaptive pixel. Each adaptive pixel is the largest pixel such that the L_p local error of the display image on it is not greater than the global error.

The merging scheme begins with a pixel mesh \mathcal{T}_n . We put \mathcal{T}_n into a first-in first-out (FIFO) queue \mathcal{Q} in an arbitrary order, and let \mathcal{M}_{δ} be empty. Note that the L_p local error of a display image on any original pixel in \mathfrak{I}_n is zero. First, we remove one pixel on the front of \mathcal{Q} , denoted by \mathbb{T}_{i}^{k} and test the L_{p} local error of the display image on it. If its L_p local error is less than or equal to the global error δ , we find its brother pixels. If all its brother pixels' L_p local errors are less than δ , we merge these four pixels into their parent pixel and put it into the rear of \mathcal{Q} . After that, we remove its brother pixels from \mathcal{Q} . If one of their L_p local error is larger than the global error, from (3.3), we know that the L_p local error of their parent pixel is also larger than the global error, which means that \mathbb{T}^k_i is an adaptive pixel. Thus, we put it into \mathcal{M}_{δ} . Otherwise, if the L_p local error of the display image on \mathbb{T}_{j}^{k} is larger than δ , then its children pixels' L_{p} local errors must be less than δ . In other words, its children pixels are adaptive pixels. This is because the pixels in \mathcal{Q} are either the original pixels or the pixels constructed by merging their children pixels, and the L_{p} local error of the display image on any original pixels is zero. Repeat this process until \mathcal{Q} is empty, in which case we output the adaptive pixel mesh \mathcal{M}_{δ} .

We next describe the merging scheme in an algorithm format. Suppose that n is a power of 2. For a given global error $\delta > 0$ and a display image u_n , the merging scheme can be described as follows.

In the initial state, \mathcal{T}_n is put into the pixel FIFO queue \mathcal{Q} in an arbitrary order, and the adaptive pixel mesh \mathcal{M}_{δ} is \emptyset .

- Step 1. If \mathcal{Q} is empty, output \mathcal{M}_{δ} and stop.
- Step 2. Remove one pixel \mathbb{T}_i^k in the head of \mathcal{Q} and conduct the following:
 - (1) If $E(u_n, \mathbb{T}_j^k)_p \leq \delta$, find the brother pixels of \mathbb{T}_i^k and perform
 - (a) If all its brother pixels' L_p local errors are less than or equal to δ , then remove the brother pixels of \mathbb{T}^k_j from \mathscr{Q} and put their parent pixel $\mathbb{T}^{k-1}_{(\lfloor \frac{j_1}{2} \rfloor, \lfloor \frac{j_2}{2} \rfloor)}$ into the rear of \mathscr{Q} .
 - (b) If one of its brother pixels' L_p local error is larger than δ , then put \mathbb{T}_i^k into \mathscr{M}_{δ} .
 - (2) If $E(u_n, \mathbb{T}_j^k)_p > \delta$, put the children pixels of \mathbb{T}_j^k into \mathcal{M}_{δ} .

Step 3. Go to Step 1.

It can be easily seen that the merging scheme is a reverse process of the basic dividing scheme studied in [7, 13, 22, 23]. The basic dividing scheme was used in [13] to partition the domain of a function in a Besov space in order to construct the best piecewise polynomial approximation on the adaptive mesh to approximate the function. Similarly, an adaptive tree process was used in [7, 22, 23] to obtain nonlinear wavelet representations of a function in a Besov space. The goal of these schemes is to construct a piecewise polynomial approximation of a function in a Besov space. The basic dividing scheme begins with a continuous domain, and it constructs an adaptive mesh by repeatedly dividing the domain. Here, we construct an adaptive mesh in a different way: the merging scheme starts with a finest uniform pixel mesh, and it generates an adaptive pixel mesh by merging pixels.

With the adaptive pixel mesh \mathcal{M}_{δ} generated by the merging scheme, we can construct an adaptive display image. Specifically, for a given global error $\delta > 0$ and a display image u_n , the adaptive display image on the adaptive pixel mesh \mathcal{M}_{δ} is defined by

$$u_{n,\delta}(\boldsymbol{x}) := \sum_{\mathbb{Q} \in \mathscr{M}_{\delta}} (\mathscr{C}_{\mathbb{Q}}^{p} u_{n}) \chi_{\mathbb{Q}}(\boldsymbol{x}). \tag{3.4}$$

In fact, as we can see from (3.4), the adaptive display image $u_{n,\delta}$ is the best L_p piecewise constant approximation of the display image u_n on the adaptive pixel mesh \mathcal{M}_{δ} .

Since the merging scheme merges brother pixels into their parent pixel, it is no doubt that the cardinality of the resulting adaptive pixel mesh is less than that of the original pixel mesh. The question is how close the adaptive display image and its original nature image can be. To answer this question, we consider the $L_p(\mathbb{T})$ error between an adaptive display image and its original natural image in Sec. 4.

4. Error of an Adaptive Display Image from its Natural Image

In this section, we estimate the $L_p(\mathbb{T})$ error between an adaptive display image $u_{n,\delta}$ and its original natural image u under the assumption that the natural image belongs to the Besov space $B_{v,\tau}^{\alpha+\varepsilon}$, for $0 < \alpha < \alpha + \varepsilon \le 1$ with $\varepsilon > 0$, 1 , $p \le v \le \infty, \ 0 < \tau \le \infty.$

We shall bound $||u - u_{n,\delta}||_p$ by estimating $||u - u_n||_p$ and $||u_n - u_{n,\delta}||_p$. The first term is the $L_p(\mathbb{T})$ error between a display image and its original natural image, while the second term is the $L_p(\mathbb{T})$ error between an adaptive display image and its original display image.

We now estimate $||u-u_n||_p$. We first establish that if a natural image $u \in L_p(\mathbb{T})$, then its corresponding display image u_n also belongs to $L_p(\mathbb{T})$. To this end, for $\mathbb{Q} \subset \mathbb{T}$ and $f \in L_p(\mathbb{Q})$, we define the average $f_{\mathbb{Q}} : L_p(\mathbb{Q}) \to \mathbb{R}$ of f on \mathbb{Q} as

$$f_{\mathbb{Q}} := \int_{\mathbb{Q}} \frac{1}{|\mathbb{Q}|} f(\boldsymbol{x}) d\boldsymbol{x}.$$

The following simple fact concerns an upper bound of the average $f_{\mathbb{O}}$.

Lemma 4.1. If $1 \leq p \leq \infty$ and $\mathbb{Q} \subset \mathbb{T}$, then for all $f \in L_n(\mathbb{Q})$,

$$|f_{\mathbb{Q}}| \le |\mathbb{Q}|^{-1/p} ||f||_{L_p(\mathbb{Q})}.$$

Proof. We prove this result by applying the Hölder inequality. For $1 \le p < \infty$, we let $p' := (1 - 1/p)^{-1}$. From the definition of $f_{\mathbb{Q}}$ and the Hölder inequality, we have that

$$|f_{\mathbb{Q}}| \leq \left| \int_{\mathbb{Q}} \frac{1}{|\mathbb{Q}|} d\mathbf{x} \right|^{1/p'} \left| \int_{\mathbb{Q}} \frac{1}{|\mathbb{Q}|} |f(\mathbf{x})|^p d\mathbf{x} \right|^{1/p}. \tag{4.1}$$

Since $\int_{\mathbb{Q}} \frac{1}{|\mathbb{Q}|} dx = 1$, it follows from (4.1) that

$$|f_{\mathbb{Q}}| \le \left| \int_{\mathbb{Q}} \frac{1}{|\mathbb{Q}|} |f(\boldsymbol{x})|^p d\boldsymbol{x} \right|^{1/p} = \frac{1}{|\mathbb{Q}|^{1/p}} ||f||_{L_p(\mathbb{Q})}.$$

For $p = \infty$, from the definition of $f_{\mathbb{Q}}$, we have that

$$|f_{\mathbb{Q}}| \le \left| \int_{\mathbb{Q}} \frac{1}{|\mathbb{Q}|} d\mathbf{x} \right| ||f||_{L_{\infty}(\mathbb{Q})} = ||f||_{L_{\infty}(\mathbb{Q})},$$

which yields the desired estimate.

We now estimate a bound on $||u_n||_p$.

Proposition 4.2. If $1 \leq p \leq \infty$ and $u \in L_p(\mathbb{T})$ is a natural image, then for all $n \in \mathbb{N}_+$, the corresponding display images u_n have the estimate

$$||u_n||_p \leq ||u||_p.$$

Proof. This is done by estimating $||u_n||_p^p$ using Lemma 4.1. From the definition of u_n and the norm $||\cdot||_p$, we have that

$$||u_n||_p^p = \int_{\mathbb{T}} \left| \sum_{\mathbf{j'} \in \mathbb{Z}_p^2} u_{\mathbf{j'}} \chi_{\mathbb{T}_{\mathbf{j'}}^{(n)}}(\mathbf{x}) \right|^p d\mathbf{x}.$$
 (4.2)

By the definition of the characteristic function, we get that

$$\sum_{\boldsymbol{j'} \in \mathbb{Z}_{-}^{2}} u_{\boldsymbol{j'}} \chi_{\mathbb{T}_{\boldsymbol{j'}}^{(n)}}(\boldsymbol{x}) = u_{\boldsymbol{j}} \quad \text{for } \boldsymbol{x} \in \mathbb{T}_{\boldsymbol{j}}^{k}.$$

$$(4.3)$$

Substituting (4.3) into (4.2) yields

$$\|u_n\|_p^p = \sum_{\boldsymbol{j} \in \mathbb{Z}_n^2} \int_{\mathbb{T}_{\boldsymbol{j}}^{(n)}} \left| \sum_{\boldsymbol{j'} \in \mathbb{Z}_2^2} u_{\boldsymbol{j'}} \chi_{\mathbb{T}_{\boldsymbol{j'}}^{(n)}}(\boldsymbol{x}) \right|^p d\boldsymbol{x} = \sum_{\boldsymbol{j} \in \mathbb{Z}_n^2} \int_{\mathbb{T}_{\boldsymbol{j}}^{(n)}} |u_{\boldsymbol{j}}|^p d\boldsymbol{x},$$

which implies

$$||u_n||_p^p = \sum_{j \in \mathbb{Z}_p^2} |u_j|^p |\mathbb{T}_j^{(n)}|.$$
 (4.4)

Since $u \in L_p(\mathbb{T})$, applying Lemma 4.1 to u_j which has the expression (3.1), we obtain that

$$|u_{j}| \le \frac{1}{|\mathbb{T}_{j}^{(n)}|^{1/p}} ||u||_{L_{p}(\mathbb{T}_{j}^{(n)})}.$$
 (4.5)

Combining (4.4) with (4.5) yields

$$||u_n||_p^p \le \sum_{j \in \mathbb{Z}_n^2} |\mathbb{T}_j^{(n)}| \frac{1}{|\mathbb{T}_j^{(n)}|} ||u||_{L_p(\mathbb{T}_j^{(n)})}^p = \sum_{j \in \mathbb{Z}_n^2} ||u||_{L_p(\mathbb{T}_j^{(n)})}^p = ||u||_p^p,$$

which completes the proof.

We recall the definition of an useful sharp maximal function $f_{\alpha,p}^{\#}$ and the smooth space $C_p^{\alpha}(\mathbb{T})$, which were introduced in [11]. For $0 < \alpha < 1$, $0 , <math>f \in L_p(\mathbb{T})$ and $x \in \mathbb{T}$, we define the sharp maximal function by

$$f_{\alpha,p}^{\#}(\boldsymbol{x}) := \sup_{\boldsymbol{x} \in \mathbb{O}} |\mathbb{Q}|^{-(\alpha/2+1/p)} E(f,\mathbb{Q})_p,$$

where the sup is taken over all squares $\mathbb{Q} \subset \mathbb{T}$ containing x. Furthermore, we recall the definition of space $C_p^{\alpha}(\mathbb{T})$ which measures smoothness of order α in $L_p(\mathbb{T})$

through the sharp maximal function $f_{\alpha,p}^{\#}$. For 0 , we say that <math>f belongs to $C_p^{\alpha}(\mathbb{T})$ if $f_{\alpha,p}^{\#} \in L_p(\mathbb{T})$. We define the seminorm

$$|f|_{C_n^{\alpha}(\mathbb{T})} := ||f_{\alpha,p}^{\#}||_p$$

and the norm

$$||f||_{C_p^{\alpha}(\mathbb{T})} := ||f||_p + |f|_{C_p^{\alpha}(\mathbb{T})}.$$

When $p = \infty$, we say that $f \in C_{\infty}^{\alpha}(\mathbb{T})$ if $f_{\alpha,1}^{\#} \in L_{\infty}(\mathbb{T})$, and define

$$|f|_{C^{\alpha}_{\infty}(\mathbb{T})} := ||f^{\#}_{\alpha,1}||_{\infty}$$

and

$$||f||_{C^{\alpha}_{\infty}(\mathbb{T})} := ||f||_{\infty} + |f|_{C^{\alpha}_{\infty}(\mathbb{T})}.$$

In fact, when p > 1 and $\alpha \in \mathbb{Z}_+$, the space $C_p^{\alpha}(\mathbb{T})$ turns out to be the Sobolev space $W_p^{\alpha}(\mathbb{T})$. For simplicity, we use the notation C_p^{α} for $C_p^{\alpha}(\mathbb{T})$.

The L_p local error of the average approximation of f on \mathbb{Q} is defined by

$$E_f(\mathbb{Q})_p := \|f - f_{\mathbb{Q}}\|_{L_p(\mathbb{Q})}.$$

For any $\mathbb{Q} \subset \mathbb{T}$ and $f \in L_p(\mathbb{Q})$, we call $\widetilde{\mathscr{C}}_{\mathbb{Q}}^p f : L_p(\mathbb{Q}) \to \mathbb{R}$ the near best L_p constant approximation of f on \mathbb{Q} if

$$||f - \widetilde{\mathscr{C}}_{\mathbb{Q}}^p f||_{L_p(\mathbb{Q})} \le c E(f, \mathbb{Q})_p$$
, for a positive constant c .

It is well-known that $f_{\mathbb{Q}}$ is the best L_2 constant approximation of f on \mathbb{Q} (see, for example, [8]). Moreover, $f_{\mathbb{Q}}$ is also a near best L_p constant approximation of f with constant 2 for $1 \leq p \leq \infty$ on \mathbb{Q} . In fact, it was proved in [8, Theorem 2] that the best L_1 constant approximation is a near best L_p constant approximation for $0 , and pointed out without proof that <math>f_{\mathbb{Q}}$ is a near best L_p constant approximation of f for $1 \leq p \leq \infty$ on \mathbb{Q} . For the completeness of this paper, we provide a proof in the following.

Proposition 4.3. If $1 \leq p \leq \infty$ and $\mathbb{Q} \subset \mathbb{T}$, then for all $f \in L_p(\mathbb{Q})$, $f_{\mathbb{Q}}$ is a near best L_p constant approximation of f on \mathbb{Q} in the sense that

$$E_f(\mathbb{Q})_p \le 2E(f,\mathbb{Q})_p.$$

Proof. This proof is done by applying Lemma 4.1 with the fact that $(f - v)_{\mathbb{Q}} = f_{\mathbb{Q}} - v$, for a constant v. We first observe that

$$||f_{\mathbb{Q}}||_{L_p(\mathbb{Q})} = \left(\int_{\mathbb{Q}} |f_{\mathbb{Q}}|^p dx\right)^{1/p} = |\mathbb{Q}|^{1/p}|f_{\mathbb{Q}}|.$$

It follows from Lemma 4.1 that

$$||f_{\mathbb{Q}}||_{L_{n}(\mathbb{Q})} \le ||f||_{L_{n}(\mathbb{Q})}.$$
 (4.6)

By the triangle inequality, we get that

$$E_f(\mathbb{Q})_p \le \|f_{\mathbb{Q}} - \mathscr{C}_{\mathbb{Q}}^p f\|_{L_p(\mathbb{Q})} + \|f - \mathscr{C}_{\mathbb{Q}}^p f\|_{L_p(\mathbb{Q})}. \tag{4.7}$$

We consider the first term on the right-hand side of (4.7). Since the average of a constant is the constant itself, for any $v \in \mathbb{R}$, we have that $(f - v)_{\mathbb{Q}} = f_{\mathbb{Q}} - v$. In particular, substituting $v := \mathscr{C}_{\mathbb{Q}}^p f$, we obtain that

$$f_{\mathbb{Q}} - \mathscr{C}_{\mathbb{Q}}^p f = (f - \mathscr{C}_{\mathbb{Q}}^p f)_{\mathbb{Q}}.$$

Combining this with (4.6) yields that

$$||f_{\mathbb{Q}} - \mathscr{C}_{\mathbb{Q}}^{p} f||_{L_{p}(\mathbb{Q})} \le ||f - \mathscr{C}_{\mathbb{Q}}^{p} f||_{L_{p}(\mathbb{Q})}. \tag{4.8}$$

Finally, substituting (4.8) into (4.7) yields that

$$E_f(\mathbb{Q})_p \le 2||f - \mathscr{C}_{\mathbb{Q}}^p f||_{L_p(\mathbb{Q})} = 2E(f, \mathbb{Q})_p,$$

proving the desired estimate.

From the definition of $f_{\alpha,p}^{\#}$, for any $\boldsymbol{x} \in \mathbb{Q}$, we have that

$$f_{\alpha,p}^{\#}(x) \ge |\mathbb{Q}|^{-(\alpha/2+1/p)} E(f,\mathbb{Q})_p.$$
 (4.9)

Combining this with Proposition 4.3 leads to the estimate

$$E_f(\mathbb{Q})_p \le 2|\mathbb{Q}|^{\alpha/2+1/p} f_{\alpha,p}^{\#}(\boldsymbol{x}). \tag{4.10}$$

Now, we are ready to give an upper bound on $||u - u_n||_p$ when $u \in C_p^{\alpha}$.

Proposition 4.4. If $0 < \alpha < 1$, $1 \le p < \infty$, and $u \in C_p^{\alpha}$ is a nature image, then there exists a positive constant c such that for all $n \in \mathbb{N}_+$,

$$||u - u_n||_p \le cn^{-\alpha} ||u||_{C_p^{\alpha}}.$$

Proof. We first comment that $u_n \in L_p(\mathbb{T})$. Because of $u \in C_p^{\alpha}$, we know that $u \in L_p(\mathbb{T})$. Hence, Proposition 4.2 ensures that $u_n \in L_p(\mathbb{T})$ as well. Since the value of u_n on $\mathbb{T}_{\boldsymbol{j}}^{(n)}$ is a constant $u_{\boldsymbol{j}}$ and $u_{\boldsymbol{j}} = u_{\mathbb{T}_{\boldsymbol{j}}^{(n)}}$, we obtain that

$$||u - u_n||_p = \left(\sum_{j \in \mathbb{Z}_n^2} E_u(\mathbb{T}_j^{(n)})_p^p\right)^{1/p}.$$
 (4.11)

We shall first show that $E_u(\mathbb{T}_{\boldsymbol{j}}^{(n)})_p$ can be bounded by $|u|_{C_p^{\alpha}(\mathbb{T}_{\boldsymbol{j}}^{(n)})}$, and then using this fact with (4.11), establish the upper bound of $||u-u_n||_p$.

Note that $u_{\alpha,p}^{\#}$ is well-defined due to $u \in L_p(\mathbb{T})$. By substituting f := u and $\mathbb{Q} := \mathbb{T}_j^{(n)}$ into (4.10), we obtain that for $\boldsymbol{x} \in \mathbb{T}_j^{(n)}$,

$$E_u(\mathbb{T}_{j}^{(n)})_p \le 2|\mathbb{T}_{j}^{(n)}|^{\alpha/2+1/p} u_{\alpha,p}^{\#}(\boldsymbol{x}).$$
 (4.12)

Notice that

$$|\mathbb{T}_{j}^{(n)}|^{1/p} E_{u}(\mathbb{T}_{j}^{(n)})_{p} = \left(\int_{\mathbb{T}_{j}^{(n)}} E_{u}(\mathbb{T}_{j}^{(n)})_{p}^{p} dx\right)^{1/p}.$$
(4.13)

Combining (4.12) and (4.13), we obtain that

$$E_{u}(\mathbb{T}_{j}^{(n)})_{p} \leq 2|\mathbb{T}_{j}^{(n)}|^{\alpha/2} \left(\int_{\mathbb{T}_{j}^{(n)}} |u_{\alpha,p}^{\#}(\boldsymbol{x})|^{p} d\boldsymbol{x} \right)^{1/p}.$$
 (4.14)

In the mean time, from the definition of $|\cdot|_{C_n^{\alpha}(\mathbb{T}_i^{(n)})}$, we have that

$$\left(\int_{\mathbb{T}_{\boldsymbol{j}}^{(n)}} |u_{\alpha,p}^{\#}(\boldsymbol{x})|^p d\boldsymbol{x}\right)^{1/p} = |u|_{C_p^{\alpha}(\mathbb{T}_{\boldsymbol{j}}^{(n)})}.$$
(4.15)

Substituting (4.15) into (4.14) yields that

$$E_u(\mathbb{T}_{j}^{(n)})_p \le 2|\mathbb{T}_{j}^{(n)}|^{\alpha/2}|u|_{C_p^{\alpha}(\mathbb{T}_{j}^{(n)})}.$$
 (4.16)

Since $|\mathbb{T}_{\boldsymbol{j}}^{(n)}| = |\mathbb{T}|n^{-2}$, combining (4.11) and (4.16), we get that

$$||u - u_n||_p \le 2|\mathbb{T}|^{\alpha/2} n^{-\alpha} \left(\sum_{j \in \mathbb{Z}_n^2} |u|_{C_p^{\alpha}(\mathbb{T}_j^{(n)})}^p \right)^{1/p}.$$
 (4.17)

Moreover, by the definition of $|\cdot|_{C_p^{\alpha}}$, we find that

$$\left(\sum_{j \in \mathbb{Z}_p^2} |u|_{C_p^{\alpha}(\mathbb{T}_j^{(n)})}^p\right)^{1/p} = |u|_{C_p^{\alpha}}.$$
(4.18)

Finally, from (4.17) and (4.18), we achieve that

$$||u - u_n||_p \le 2|\mathbb{T}|^{\alpha/2}n^{-\alpha}|u|_{C_n^{\alpha}} \le cn^{-\alpha}||u||_{C_n^{\alpha}},$$

where
$$c = 2|\mathbb{T}|^{\alpha/2}$$
.

Indeed, $C_p^{\alpha}(\mathbb{T})$ is a natural extension of the Sobolev space $W_p^{\alpha}(\mathbb{T})$, which was discussed in [12]. The result of the $L_p(\mathbb{T})$ error between a function in the Sobolev space and its best piecewise constant approximation on a non-uniform partition mesh is well-known. For example, in [21] (see Theorem 6.1), it was proved that

for any non-uniform partition $\triangle := \{a = x_0 < x_1 < \dots < x_{n-1} < x_n = b\}$, if $1 \le p \le q \le \infty$ and $f \in W^1_p[a,b]$, then

$$\inf_{c \in \mathbb{R}^n} \left\| f - \sum_{j \in \mathbb{Z}_n} c_j \chi_{\Delta_j^{(n)}} \right\|_q \le \bar{\triangle}^{-(1-1/p+1/q)} \|f\|_{W_p^1[a,b]},$$

where $\mathbf{c} := \{c_j\}_{j \in \mathbb{Z}_n} \in \mathbb{R}^n$, $\triangle_j^{(n)} := [x_j, x_{j+1})$ and $\bar{\triangle} := \max_{j \in \mathbb{Z}_n} (x_{j+1} - x_j)$. Now, we turn to estimating $||u_n - u_{n,\delta}||_p$.

Proposition 4.5. If $1 and <math>0 < \alpha < \min(1, 2 - 2/p)$, then there exists a positive constant c such that for all $\delta > 0$, $n = 2^k$, $k \in \mathbb{N}_+$, natural images $u \in C_p^{\alpha}$, their corresponding display images u_n and adaptive display images $u_{n,\delta}$,

$$||u_n - u_{n,\delta}||_p < c|\mathcal{M}_{\delta}|^{-\alpha/2}||u||_{C_n^{\alpha}}.$$

Proof. We first comment that u, u_n and $u_{n,\delta}$ all belong to $L_p(\mathbb{T})$ if $u \in C_p^{\alpha}$. Clearly, we know that $u \in C_p^{\alpha}$ implies $u \in L_p(\mathbb{T})$. Besides, by Proposition 4.2, we have that $u_n \in L_p(\mathbb{T})$ as well. In addition, from the merging scheme, we know that

$$||u_n - u_{n,\delta}||_p = \left(\sum_{\mathbb{Q} \in \mathcal{M}_{\delta}} E(u_n, \mathbb{Q})_p^p\right)^{1/p} \le (|\mathcal{M}_{\delta}|\delta^p)^{1/p},$$

which implies

$$||u_n - u_{n,\delta}||_p \le |\mathcal{M}_{\delta}|^{1/p} \delta. \tag{4.19}$$

Thus, combining the triangle inequality and (4.19), we have that

$$||u_{n,\delta}||_p \le ||u_n||_p + ||u_n - u_{n,\delta}||_p < \infty,$$

which implies $u_{n,\delta} \in L_p(\mathbb{T})$.

For any adaptive pixel $\mathbb{Q} \in \mathcal{M}_{\delta}$, from the merging scheme, we know that its parent pixel \mathbb{Q}' satisfies

$$E(u_n, \mathbb{Q}')_p > \delta. \tag{4.20}$$

Furthermore, from the definition of $E(u_n, \mathbb{Q}')_p$, we have that

$$E(u_n, \mathbb{Q}')_p \le \|u_n - \mathscr{C}^p_{\mathbb{Q}'} u\|_{L_p(\mathbb{Q}')}. \tag{4.21}$$

Since $\mathscr{C}^p_{\mathbb{Q}'}u$ is a constant, according to Proposition 4.2, we get that

$$||u_n - \mathscr{C}_{\mathbb{Q}'}^p u||_{L_p(\mathbb{Q}')} \le E(u, \mathbb{Q}')_p. \tag{4.22}$$

Therefore, combining (4.20)–(4.22), we obtain that

$$\delta < E(u, \mathbb{Q}')_p. \tag{4.23}$$

By (4.9), for any $x \in \mathbb{Q}'$, we have that

$$|\mathbb{Q}'|^{-(\alpha/2+1/p)}E(u,\mathbb{Q}')_p \le u_{\alpha,p}^{\#}(x).$$
 (4.24)

Let $q := (\alpha/2 + 1/p)^{-1}$. Note that $|\mathbb{Q}'| = 4|\mathbb{Q}|$. Then for any $\boldsymbol{x} \in \mathbb{Q}$, combining (4.23) and (4.24), we get that

$$\delta < 4^{1/q} |\mathbb{Q}|^{1/q} u_{\alpha,p}^{\#}(x).$$
 (4.25)

Because of $u \in C_p^{\alpha}$, we know that $u_{\alpha,p}^{\#} \in L_p(\mathbb{T})$. Since $0 < \alpha < \min(1, 2 - 2/p)$, it can be seen easily that $1 < q = (\alpha/2 + 1/p)^{-1} < p$. According to the Hölder inequality, we get that $u_{\alpha,p}^{\#} \in L_q(\mathbb{T})$ and

$$||u_{\alpha,p}^{\#}||_{q} \le |\mathbb{T}|^{1/q-1/p}||u_{\alpha,p}^{\#}||_{p}. \tag{4.26}$$

Furthermore, from (4.25), we have that

$$|\mathbb{Q}|^{1/q} \delta = \left(\int_{\mathbb{O}} \delta^q \mathrm{d} \boldsymbol{x} \right)^{1/q} < \left(\int_{\mathbb{O}} 4|\mathbb{Q}| |u_{\alpha,p}^{\#}(\boldsymbol{x})|^q \mathrm{d} \boldsymbol{x} \right)^{1/q} = 4^{1/q} |\mathbb{Q}|^{1/q} \|u_{\alpha,p}^{\#}\|_{L_q(\mathbb{Q})},$$

which implies that

$$\delta < 4^{1/q} \| u_{\alpha,p}^{\#} \|_{L_q(\mathbb{Q})}.$$
 (4.27)

Note that (4.27) is true for any $\mathbb{Q} \in \mathcal{M}_{\delta}$. Therefore, from the definition of C_p^{α} norm, combining (4.26) and (4.27), we achieve that

$$\begin{aligned} |\mathcal{M}_{\delta}|\delta^{q} &= \sum_{\mathbb{Q} \in \mathcal{M}_{\delta}} \delta^{q} < 4 \sum_{\mathbb{Q} \in \mathcal{M}_{\delta}} \|u_{\alpha,p}^{\#}\|_{L_{q}(\mathbb{Q})}^{q} = 4 \|u_{\alpha,p}^{\#}\|_{q}^{q} \\ &\leq 4 |\mathbb{T}|^{1-q/p} \|u_{\alpha,p}^{\#}\|_{p}^{q} \leq 4 |\mathbb{T}|^{1-q/p} \|u\|_{C_{\alpha}^{\alpha}}^{q}, \end{aligned}$$

which yields

$$\delta < 4^{1/q} |\mathbb{T}|^{1/q - 1/p} |\mathcal{M}_{\delta}|^{-1/q} ||u||_{C_{\nu}^{\alpha}}. \tag{4.28}$$

Since $1/p - 1/q = -\alpha/2$, combining (4.19) and (4.28), we observe that

$$||u_n - u_{n,\delta}||_p < |\mathcal{M}_{\delta}|^{1/p} 4^{1/q} |\mathbb{T}|^{1/q - 1/p} |\mathcal{M}_{\delta}|^{-1/q} ||u||_{C_p^{\alpha}} = c |\mathcal{M}_{\delta}|^{-\alpha/2} ||u||_{C_p^{\alpha}},$$

where
$$c := 4^{1/q} |\mathbb{T}|^{-\alpha/2}$$
.

Now, we are going to show that $B_{v,\tau}^{\alpha+\varepsilon}$ is continuously embedded in C_p^{α} . We use the notation $A \hookrightarrow B$ to denote space A is continuously embedded in B. We recall a well-known Besov embedding, which can be found in [10]. If $0 < \alpha < \alpha + \varepsilon \leq 1$ with $\varepsilon > 0$, $0 and <math>0 < \tau, q \leq \infty$, then the following continuous embedding holds

$$B_{p,\tau}^{\alpha+\varepsilon} \hookrightarrow B_{p,q}^{\alpha}.$$

According to the Hölder inequality, we have that if $0 < \alpha < \alpha + \varepsilon \le 1$ with $\varepsilon > 0$, $1 \le p \le v \le \infty$ and $0 < \tau, q \le \infty$, then the following continuous embedding

holds:

$$B_{v,\tau}^{\alpha+\varepsilon} \hookrightarrow B_{p,q}^{\alpha}.$$
 (4.29)

From (4.29), we can immediately derive that if $0 < \alpha < \alpha + \varepsilon \le 1$ with $\varepsilon > 0$, $0 < \tau \le \infty$ and $1 \le p \le v \le \infty$, then

$$B_{v,\tau}^{\alpha+\varepsilon} \hookrightarrow B_{p,p}^{\alpha}.$$
 (4.30)

In addition, a continuous embedding theorem about C_p^{α} was proved in [11] (see [11, Theorem 7.1]). If $\alpha > 0$ and $1 \le p \le \infty$, then the following continuous embeddings hold:

$$B_{p,p}^{\alpha} \hookrightarrow C_p^{\alpha} \hookrightarrow B_{p,\infty}^{\alpha}.$$
 (4.31)

Combining (4.30) and (4.31), we find that if $0 < \alpha < \alpha + \varepsilon \le 1$ with $\varepsilon > 0$, $0 < \tau \le \infty$ and $1 \le p \le v \le \infty$, then

$$B_{v,\tau}^{\alpha+\varepsilon} \hookrightarrow C_p^{\alpha}.$$
 (4.32)

In particular, for any function $f \in B_{v,\tau}^{\alpha+\varepsilon}$, there exists a positive constant c such that

$$||f||_{C_n^{\alpha}} \le c||f||_{B_n^{\alpha+\varepsilon}}. \tag{4.33}$$

Finally, we are ready to estimate $||u - u_{n,\delta}||_p$.

Theorem 4.6. If $1 , and <math>u \in B_{v,\tau}^{\alpha+\varepsilon}$ is a nature image for $0 < \alpha < \alpha+\varepsilon \le \min(1, 2-2/p)$ with $\varepsilon > 0$, $p \le v \le \infty$ and $0 < \tau \le \infty$, then there exists a positive constant c such that for all $\delta > 0$, $n = 2^k, k \in \mathbb{N}_+$,

$$||u - u_{n,\delta}||_p < c(n^{-\alpha} + |\mathcal{M}_{\delta}|^{-\alpha/2})||u||_{B_{\alpha}^{\alpha+\varepsilon}}.$$

Proof. By the triangle inequality, we have that

$$||u - u_{n,\delta}||_p \le ||u - u_n||_p + ||u_n - u_{n,\delta}||_p.$$
(4.34)

From the embedding relation (4.32), we know that $u \in B_{v,\tau}^{\alpha+\varepsilon}$ implies $u \in C_p^{\alpha}$. Therefore, by Propositions 4.4 and 4.5, we have the upper bound of the first term and the second term of the right-hand side of (4.34), respectively. Substituting them into (4.34) and combining the resulting estimate with (4.33), we prove the desired result.

It was found in [3] that many natural images belong to the Besov space $B_{2,\infty}^{\alpha}$ with $0 < \alpha < 1$. Note that $B_{2,\infty}^{\alpha}$ is a special case of $B_{2,\tau}^{\alpha+\varepsilon}$. Indeed, according to Theorem 4.6, we have the following corollary.

Corollary 4.7. If $u \in B_{2,\tau}^{\alpha+\varepsilon}$ is a nature image for $0 < \alpha < \alpha + \varepsilon \le 1$ with $\varepsilon > 0$ and $0 < \tau \le \infty$, then there exists a positive constant c such that for all $\delta > 0$, $n = 2^k$, $k \in \mathbb{N}_+$,

$$||u - u_{n,\delta}||_2 < c(n^{-\alpha} + |\mathcal{M}_{\delta}|^{-\alpha/2})||u||_{B_2^{\alpha+\varepsilon}}.$$

Proof. This is a special case of Theorem 4.6 with v = p = 2.

5. Numerical Experiments

We present in this section numerical experimental results to verify that the visual quality of the adaptive display image is comparable with that of its original display image while the cardinality of the adaptive pixel mesh is significantly less than that of the original pixel mesh.

We choose the testing display images from SAMPLING archive (8 bit) of "TESTIMAGES" database introduced in [2], whose purpose is providing "natural" images to test resampling algorithms. Here, "natural" means capturing by camera directly and without artificial processing. The original resolution of the display images in this database is 2400. In order to get 2048×2048 display images, we select the central 2048×2048 region of each display image. In what follows, we choose p=2. Matlab R2013b is used to run all the experiments presented in this section.

The first experiment is to show that the cardinality of the adaptive pixel mesh is significantly less than that of the original pixel mesh, while the corresponding adaptive display images have comparable quality with the original display images. We choose from the database three display images which have low degrees of smoothness. The first one is "Flowers" which represents the natural objects. The second one is "Building" which represents the man-made building. The third one is "Clips" which represents the messy man-made things. All of these images have significant amount of edges. In order to show the adaptive pixel mesh clearly, we choose the highest resolution 2048×2048 display images. In our adaptive merging scheme, the global error δ is chosen to be 0.01. The experimental results are shown in Fig. 1. As shown in this Fig. 1, the quality of the resulting adaptive display images is comparable to that of the corresponding original display images, while the cardinalities of all these three adaptive pixel meshes are significantly less than those of the corresponding original pixel meshes. In fact, one cannot tell the difference between these display images and their corresponding adaptive display images. Last but not least, the adaptive pixel mesh is dense around the edges of a display image. This feature can be used for edge detection or image segmentation.

The next experiment is to test the effect of the global error δ on the adaptive display image. For this experiment, we again choose the three 2048×2048 display images tested in the previous experiment. We choose different δ ($\delta = 0.1, 0.5$ and 1.0) and show the difference among the reconstructed adaptive display images. Results of this experiment are shown in Fig. 2. We can observe from Fig. 2 that the size of the adaptive pixel depends on δ . The larger the δ is chosen, the bigger the adaptive pixel's size is and the fewer the cardinality of the adaptive pixel mesh has. However, with the increasing of δ , the display images become more and more blurred. But we still can see the outline of these adaptive display images. Therefore, the visual quality of the adaptive display image depends on δ . If one wants to generate an adaptive display image with better quality, it is suggested to choose a smaller value for δ .

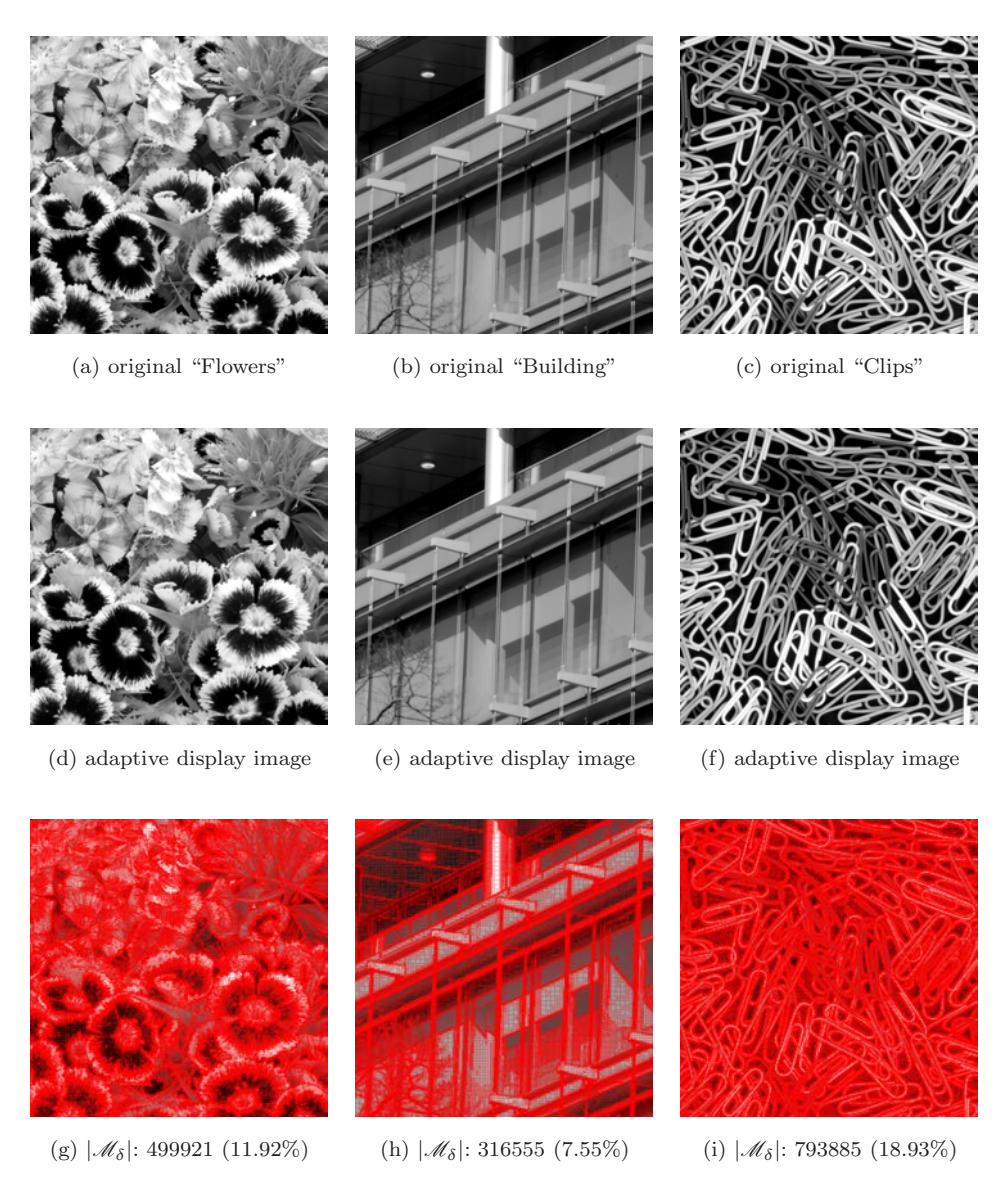


Fig. 1. The display image, the corresponding adaptive display image and adaptive pixel mesh of "Flowers", "Building" and "Clips". (a)–(c) are the display images with resolution 2048; (d)–(f) are the adaptive display images of (a)–(c) produced by the adaptive merging scheme with $\delta=0.01$ and n=2048; (g)–(i) are the adaptive pixel mesh of (a)–(c), respectively. The percentage in (g)–(i) is the ratio of $|\mathcal{M}_{\delta}|$ to n^2 .

The last experiment is to compare the $L_2(\mathbb{T})$ error $||u-u_n||_2$ with $||u-u_{n,\delta}||_2$. For generality of this experiment, we test all 40 display images in SAMPLING archive of "TESTIMAGES" database. For the comparison purpose, we take display images with resolution 2048 as natural images u and obtain their 512×512 display

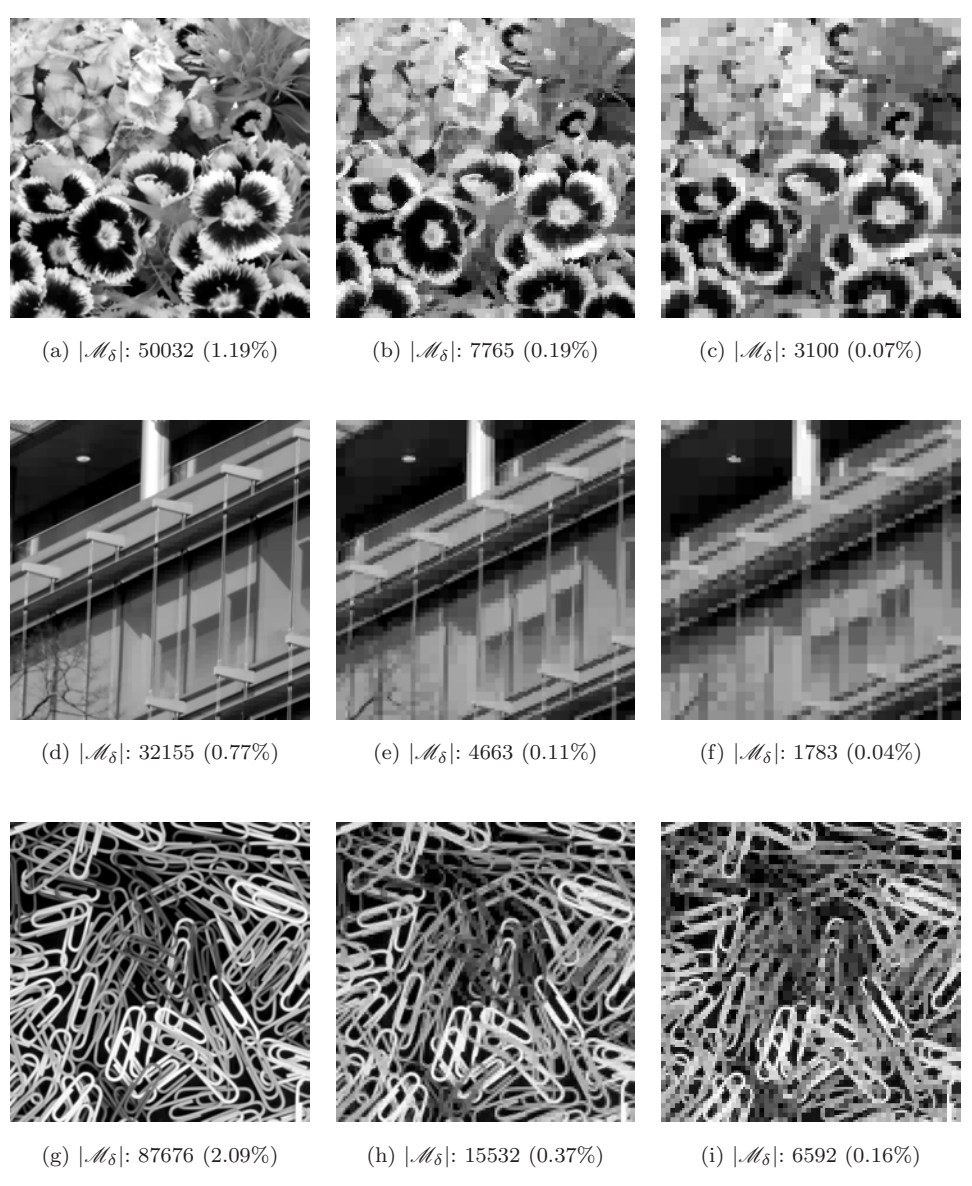


Fig. 2. Adaptive display images of "Flowers", "Building" and "Clips" with different δ . The resolution of display images is n=2048. From left to right, δ is 0.1, 0.5 and 1.0. The percentage in each subfigure is the ratio of $|\mathcal{M}_{\delta}|$ to n^2 .

images u_n by averaging the corresponding pixel values. We then construct adaptive display images $u_{n,\delta}$ from these display images by using the adaptive merging scheme with $\delta = 0.01$. We calculate the relative errors

$$\operatorname{Err1} := \frac{\|u - u_n\|_2}{\|u\|_2}, \quad \operatorname{Err2} := \frac{\|u - u_{n,\delta}\|_2}{\|u\|_2}, \quad \operatorname{Err3} := \frac{\|u_n - u_{n,\delta}\|_2}{\|u\|_2}$$

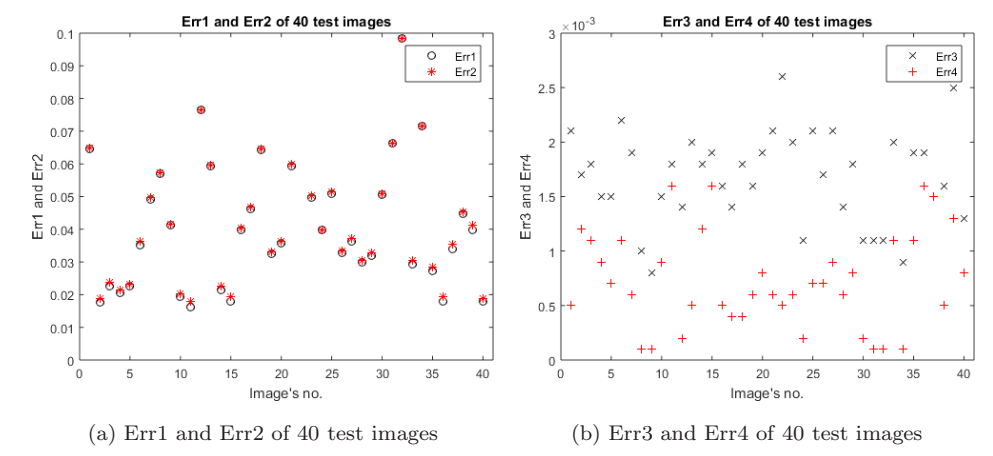


Fig. 3. (Color line) Err1, Err2, Err3 and Err4 of 40 test images in "TESTIMAGES". The resolution of display images is n=512 and $\delta=0.01$. (a) Comparison of Err1 and Err2. The black circle point is the Err1 of test images while the red star point is Err2. (b) Comparison of Err3 and Err4. The black cross point is the Err3 of test images while the red plus point is Err4.

Table 1. Err1, Err2, Err3 and Err4 of 40 test images in "TESTIMAGES" (part 1). The resolution of display images is n=512. $|\mathcal{M}_{\delta}|$ is the cardinality of adaptive pixel mesh with $\delta=0.01$, and the percentages are the ratio of $|\mathcal{M}_{\delta}|$ to n^2 .

Display image	$ \mathscr{M}_{\delta} $	Err1	Err2	Err3	Err4
Almonds	214885 (81.97%)	0.0645	0.0650	0.0021	0.0005
Apples	124120 (47.35%)	0.0175	0.0187	0.0017	0.0012
Baloons	111337 (42.47%)	0.0226	0.0237	0.0018	0.0011
Bananas	112975 (43.10%)	0.0205	0.0214	0.0015	0.0009
Billiard balls (a)	77770 (29.67%)	0.0226	0.0233	0.0015	0.0007
Billiard balls (b)	119356 (45.53%)	0.0352	0.0363	0.0022	0.0011
Building	123757 (47.21%)	0.0492	0.0498	0.0019	0.0006
Cards (a)	151315 (57.72%)	0.0571	0.0572	0.0010	0.0001
Cards (b)	106486 (40.62%)	0.0413	0.0414	0.0008	0.0001
Carrots	148726 (56.73%)	0.0193	0.0202	0.0015	0.0009
Chairs	55297 (21.09%)	0.0162	0.0178	0.0018	0.0016
Clips	219733 (83.82%)	0.0764	0.0766	0.0014	0.0002
Coins	194665 (74.26%)	0.0592	0.0597	0.0020	0.0005
Cushions	99748 (38.05%)	0.0214	0.0226	0.0018	0.0012
Ducks	75157 (28.67%)	0.0179	0.0195	0.0019	0.0016
Fence	151342 (57.73%)	0.0399	0.0404	0.0016	0.0005
Flowers	194857 (74.33%)	0.0463	0.0467	0.0014	0.0004
Garden table	208999 (79.73%)	0.0642	0.0646	0.0018	0.0004
Guitar bridge	182884 (69.76%)	0.0326	0.0332	0.0016	0.0006
Guitar fret	134284 (51.23%)	0.0356	0.0364	0.0019	0.0008

and

$$Err4 := Err2 - Err1.$$

The numerical results are presented in Fig. 3, Tables 1 and 2. It can be seen from these results that for all 40 test images, Err1 is comparable to Err2, and both Err3

Display image	$ \mathcal{M}_{\delta} $	Err1	Err2	Err3	Err4
Guitar head	185704 (70.84%)	0.0594	0.0600	0.0021	0.0006
Keyboard (a)	159883 (60.99%)	0.1135	0.1140	0.0026	0.0005
Keyboard (b)	172699 (65.88%)	0.0496	0.0502	0.0020	0.0006
Lion	128749 (49.11%)	0.0397	0.0399	0.0011	0.0002
Multimeter	172216 (65.70%)	0.0508	0.0515	0.0021	0.0007
Pencils (a)	153400 (58.52%)	0.0327	0.0334	0.0017	0.0007
Pencils (b)	151510 (57.80%)	0.0362	0.0371	0.0021	0.0009
Pillar	141163 (53.85%)	0.0298	0.0304	0.0014	0.0005
Plastic	209938 (80.08%)	0.0319	0.0327	0.0018	0.0008
Roof	138412 (52.80%)	0.0507	0.0509	0.0011	0.0002
Scarf	243634 (92.94%)	0.0662	0.0663	0.0011	0.0001
Screws	229780 (87.65%)	0.0984	0.0985	0.0011	0.0001
Snails	130390 (49.74%)	0.0293	0.0304	0.0020	0.0011
Socks	251896 (96.09%)	0.0716	0.0717	0.0009	0.0001
Sweets	137257 (52.36%)	0.0273	0.0284	0.0019	0.0010
Tomatoes (a)	120379 (45.92%)	0.0178	0.0194	0.0019	0.0016
Tomatoes (b)	100624 (38.39%)	0.0340	0.0355	0.0026	0.0015
Tools (a)	195217 (74.47%)	0.0448	0.0453	0.0016	0.0005
Tools (b)	154963 (59.11%)	0.0399	0.0412	0.0025	0.0013
Wood game	94612 (36.09%)	0.0179	0.0187	0.0013	0.0008

Table 2. Err1, Err2, Err3 and Err4 of 40 test images in "TESTIMAGES" (part 2). The resolution of display images is n=512. $|\mathcal{M}_{\delta}|$ is the cardinality of adaptive pixel mesh with $\delta=0.01$, and the percentages are the ratio of $|\mathcal{M}_{\delta}|$ to n^2 .

and Err4 are closed to zero while the cardinality of the adaptive pixel mesh is less than that of the original pixel mesh. Besides, we can see from Tables 1 and 2 that the adaptive merging scheme is suitable for those images which have simple backgrounds or simple patterns such as "Chairs" and "Ducks", but less suitable for texture images, like "Scarf" and "Socks".

From the three experiments presented above, we conclude that the cardinality of the adaptive pixel mesh produced by the adaptive merging scheme can be significantly less than that of the original pixel mesh, with preserving a comparable image quality. Furthermore, the proposed adaptive reconstruction method is more suitable for images having simple backgrounds or simple patterns.

6. Conclusions

In this paper, we develop an adaptive reconstruction method for display images. The method employs an adaptive merging scheme which constructs an adaptive pixel mesh from the pixel mesh of a display image. The cardinality of the adaptive pixel mesh can be significantly less than that of the original pixel mesh, while the resulting adaptive display image has an image quality comparable to that of the original display image. We have established that the adaptive display image constructed based on the adaptive pixel mesh is the best L_p piecewise constant approximation of its original display image. By assuming that natural images belong to Besov spaces, we estimate the $L_p(\mathbb{T})$ error between the adaptive display image

Acknowledgments

This work was supported in part by the Special Project on High-performance Computing under the National Key R&D Program (No. 2016YFB0200602), by US National Science Foundation under grant DMS-1912958, by Natural Science Foundation of China under grant 11771464. The first author is also supported by 2018NFGD under grant 20186700031680001. The second author is also a professor emeritus, Department of Mathematics, Syracuse University, Syracuse, NY 13244, USA; and a retired professor, School of Data and Computer Science, Guangdong Provincial Key Laboratory of Computational Science, Sun Yat-Sen University, Guangzhou 510275, P. R. China.

References

- L. Alvarez, Y. Gousseau and J. M. Morel, Scales in natural images and a consequence on their bounded variation norm, *Int. Conf. Scale-Space Theories in Computer Vision* (Springer, Berlin, Heidelberg, 1999), pp. 247–258.
- [2] N. Asuni and A. Giachetti, TESTIMAGES: A Large-scale archive for testing visual devices and basic image processing algorithms, *The Eurographics Association* (Strasbourg, France, 2014), pp. 63–70.
- [3] A. S. Carasso, Singular integrals, image smoothness, and the recovery of texture in image deblurring, SIAM J. Appl. Math. 64 (2004) 1749–1774.
- [4] A. Chambolle, R. A. DeVore, N. Y. Lee and B. J. Lucier, Nonlinear wavelet image processing: Variational problems, compression, and noise removal through wavelet shrinkage, *IEEE Trans. Image Process.* 7 (1998) 319–335.
- [5] A. Chambolle and B. J. Lucier, Interpreting translation-invariant wavelet shrinkage as a new image smoothing scale space, *IEEE Trans. Image Process.* 10 (2001) 993– 1000.
- [6] T. F. Chan and J. J. Shen, Image Processing and Analysis: Variational, PDE, Wavelet, and Stochastic Methods (Society for Industrial and Applied Mathematics, Philadelphia, 2005).
- [7] W. Dahmen, R. Schneider and Y. Xu, Nonlinear functionals of wavelet expansionsadaptive reconstruction and fast evaluation, *Numer. Math.* 86 (2000) 49–101.
- [8] R. A. DeVore, B. Jawerth and B. J. Lucier, Image compression through wavelet transform coding, *IEEE Trans. Inform. Theory* 38 (1992) 719–746.
- R. A. DeVore and B. J. Lucier, Fast wavelet techniques for near-optimal image processing, *IEEE Military Communications Conference*, 1992 (MILCOM'92), Conf. Record (IEEE, San Dieg., California, 1992), pp. 1129–1135.
- [10] R. A. DeVore and B. J. Lucier, Classifying the smoothness of images: Theory and applications to wavelet image processing, Proc. 1st Int. Cof. Image Processing, 1994 (ICIP-94), IEEE, Austin, TX, Vol. 2 (IEEE, 1994), pp. 6–10.
- [11] R. A. DeVore and R. C. Sharpley, *Maximal Functions Measuring Smoothness* (American Mathematical Society, Providence, RI, 1984).
- [12] R. A. DeVore, R. C. Sharpley and S. D. Riemenschneider, n-Widths for C_p^{α} spaces, in Anniversary Volume on Approximation Theory and Functional Analysis (Birkhäuser, Basel, 1984), pp. 213–222.

- [13] R. A. DeVore and X. M. Yu, Degree of adaptive approximation, Math. Comput. 55 (1990) 625–635.
- [14] J. B. Garnett, T. M. Le, Y. Meyer and L. A. Vese, Image decompositions using bounded variation and generalized homogeneous Besov spaces, Appl. Comput. Harmon. Anal. 23 (2007) 25–56.
- [15] Y. Gousseau and J. M. Morel, Are natural images of bounded variation? SIAM J. Math. Anal. 33 (2001) 634–648.
- [16] A. Hornberg, Handbook of Machine Vision (Wiley-VCH Veriag GmbH & Co KGaA, Weinheim, 2006).
- [17] E. H. Lieb and M. Loss, Analysis, 2nd edn. (American Mathematical Society Providence, RI, 2001).
- [18] Y. Meyer, Oscillating Patterns in Image Processing and Nonlinear Evolution Equations: The Fifteenth Dean Jacqueline B. Lewis Memorial Lectures (American Mathematical Society, Providence, RI, 2001).
- [19] M. Nikolova, Local strong homogeneity of a regularized estimator, SIAM J. Appl. Math. 61 (2000) 633–658.
- [20] L. I. Rudin, S. Osher and E. Fatemi, Nonlinear total variation based noise removal algorithms, *Physica D, Nonlinear Phenom.* 60 (1992) 259–268.
- [21] L. L. Schumaker, Spline Functions: Basic Theory, 3rd edn. (Cambridge University Press, Cambridge, New York, Melbourne, Mabrid, Cape Town, Singapore, Sao Paulo, 2007).
- [22] Y. Xu and Q. Zou, Adaptive wavelet methods for elliptic operator equations with nonlinear terms, Adv. Comput. Math. 19 (2003) 99–146.
- [23] Y. Xu and Q. Zou, Tree wavelet approximations with applications, Sci. China Ser. A, Math. 48 (2005) 680–702.